

Influence of control parameters on synchronization stability of virtual synchronous generator

YANXIA ZHANG , YACHAO CHENG, KAIXIANG LIU, YUE HAN

*School of Electrical and Information Engineering, Tianjin University
China*

e-mail: zyx1962@tju.edu.cn

(Received: 25.10.2021, revised: 10.06.2022)

Abstract: Different from the synchronization mechanism of synchronous generators, the non-synchronous generators must be synchronized with the grid through a controller. Generally, the virtual synchronous generator (VSG) control strategy is adopted for this purpose. In view of the current situation, where the control loops are not comprehensively considered in the research of the synchronization stability of the VSG, this paper considers multiple control loops, such as active frequency loops, virtual governors, power filters and current constraint control, to establish the mathematical model of the VSG and infinite system. On this basis, the correlation formula between power angle difference and control parameters is deduced. Adopting the phase plane method, the influence of different control loops and their parameters on the transient synchronization stability is analyzed. Finally, a setting principle of the frequency modulation coefficient of virtual governors is proposed, which not only meets the response speed of control systems, but also has good control performance.

Key words: control parameters, frequency modulation coefficient, phase plane method, synchronization stability, virtual synchronous generator

1. Introduction

Distributed energy, also known as a non-synchronous generator [1], has the characteristics of randomness and volatility. When coupled with the development of DC transmission technology, the power system is not only the “physical synchronization” dominated by synchronous generators (SGs) any longer, but also the “controlled synchronization” participated by power electronic components [2]. This makes the stability of power systems facing a great challenge. The out-of-step of non-synchronous generators includes three types: the power synchronization loop (PSL) out-of-step, phase-locked loop (PLL) out-of-step, and out-of-step caused by time delay



© 2022. The Author(s). This is an open-access article distributed under the terms of the Creative Commons Attribution-NonCommercial-NoDerivatives License (CC BY-NC-ND 4.0, <https://creativecommons.org/licenses/by-nc-nd/4.0/>), which permits use, distribution, and reproduction in any medium, provided that the Article is properly cited, the use is non-commercial, and no modifications or adaptations are made.

accumulation of each control loop [3]. Among them, the PSL mainly includes power droop control and virtual synchronous generator (VSG) control [4], and the latter has a wider application. When the VSG is applied, an inverter can provide inertial support for the grid by simulating the external characteristics of the SG using the core control with an active frequency loop and reactive voltage loop. At present, research on the synchronization stability of the VSG with a small disturbance has been relatively advanced, while that on the transient synchronization stability is still in the stage of continuous exploration. Therefore, it is of great theoretical significance and practical value to deeply study the transient synchronization stability of the VSG to ensure the safe and stable operation of power systems.

The traditional methods to analyze transient synchronization stability mainly include the numerical simulation method, equal area criteria (EAC), and Lyapunov function method. Reference [5] analyzed the synchronization stability of the VSG with the numerical simulation method, and considered mainly the influence of active frequency loops. The research object of Reference [6] is the grid-connected inverter based on droop control, which can be regarded as a special VSG with zero rotational inertia [7]. When establishing the mathematical model, the author considers the active frequency loop and reactive voltage loop, but does not consider the virtual governor, power filters and current constraint control. Reference [8] overviewed the synchronization stability of the grid-following inverter and grid-forming inverter, and proposed a scheme to improve the synchronization stability by optimizing the control link and adjusting the control parameters. However, the inverter adopts the same droop control strategy as reference [6], so there is still the problem that the control loops are not considered comprehensively. Reference [9] considered the influence of the reactive voltage loop on the VSG additionally, constructed the Lyapunov function to analyze its synchronization stability, but the premise that the response speed of the reactive voltage loop is much faster than that of the active frequency loop may not be met by different VSGs [10]. References [11, 12] are the work of the same research group, the former proposed utilizing virtual impedance control to limit the fault current, the latter pointed out that virtual impedance control is superior to the current saturation algorithm in transient stability and inferior to the saturation algorithm in current limiting. Therefore, the hybrid current limiting control combining the advantages of both is proposed, whose disadvantage is that power filters, virtual governor and the virtual inertia of the active frequency loop are not considered. Reference [13] pointed out that the VSG is more prone to transient instability when considering the current limiter. The reason is that the current limiter offsets the power angle curve and reduces the critical clearing angle. This paper adopted the SEPFC (stability enhanced P-f droop control) method to improve the active frequency loop. Reference [14] approximated the transient output current of the VSG based on the Sigmoid function and analyzed its synchronization stability with the Lyapunov function. Reference [15] established linearized and nonlinearized models of the VSG. The authors combined the two to analyze the synchronization stability of the VSG and used the transient damping method to improve the active frequency loop. Based on references [15, 16], the authors analyzed the effect of the reactive voltage loop on the synchronization stability, which pointed out that the power filter with a lower cutoff frequency is beneficial to improve the transient stability. The disadvantage is that the control loops of the VSG are not fully considered. Reference [17] established a model of a VSG and an inverter with a PLL connected to a power grid in parallel, and used EAC to analyze the influence of controlled current on the transient synchronization stability of the VSG.

To sum up, in terms of analysis objects, the control loops of the VSG are not fully considered. In addition to the active frequency loop and reactive voltage loop, the VSG also includes other control loops such as virtual governors, power filters and current constraint control. Only by comprehensively considering these control loops to establish a mathematical model of the VSG, it can be more practical to study the synchronization stability. In terms of the analysis method, the EAC completely ignores the damping coefficient of the VSG, which is too conservative to analyze the transient synchronization stability. Lyapunov functions for the VSG are still rarely reported. The numerical simulation method is considered to be the most advanced and reliable method [4, 18]. This paper comprehensively considers multiple control loops such as active frequency loops, virtual governors, power filters and current constraint control, to establish the mathematical model of the VSG, considering the effect of virtual governors on equivalent damping coefficients, current constraint control on output power and the time constant of power filters on equivalent electromagnetic torque. On this basis, the correlation formula between power angle difference and control parameters is deduced. Adopting the phase plane method, the influence of multiple control loops on the transient synchronization stability of the VSG is analyzed. Considering that the introduction of virtual governor increases the equivalent damping coefficient, starting with the virtual governor, this paper proposes the setting principle of the frequency modulation coefficient which not only meets the response speed of the control system but also has a good control effect. The rest of this paper is organized as follows: In Section 2, the mathematical model of the VSG, considering only the core control loop, is given. In Section 3, the mathematical model of the main control loops is studied. In Section 4, the mathematical model of the VSG, considering multiple control loops, is established and the correlation formula between the power angle difference and control parameters is deduced. In Section 5, the influence of multiple control loops on the transient synchronization stability of the VSG is analyzed by the phase plane method, and a setting principle of the frequency modulation coefficient of the virtual governor is proposed. In Section 6, the conclusions are summarized.

2. Mathematical model of VSG considering only the core control loop

The topology of a typical VSG and its equivalent relationship with a SG are shown in Fig. 1. The new energy generation unit and the DC-side power are equivalent to the prime mover (PM) [19]; $E \angle \theta$ is the port voltage of the VSG, which is equivalent to the potential in the SG; L_f is the inductance of the LC filter at the outlet of the VSG, equivalent to that of the SG, with a current of $I_f \angle \theta_f$; C_f is the capacitance of the LC filter, whose capacitance voltage $U_c \angle \theta_c$ is equivalent to the terminal voltage of the SG. L_g is the sum of the transformer and the transmission line equivalent inductance, i.e., L_T and L_l ; $U_g \angle \theta_g$ is the infinite bus voltage. The power angle difference between the VSG and the infinity system is $\delta = \theta - \theta_g$; ω and ω_g are their angular velocity, whose difference is $\Delta\omega$. The relationship between δ and $\Delta\omega$ is

$$\frac{d\delta}{dt} = \Delta\omega = \omega - \omega_g. \quad (1)$$

The core control of Fig. 1 is shown in Fig. 2. The active frequency loop and the reactive voltage loop provide the phase angle value and rms voltage value, respectively, which are vectorially

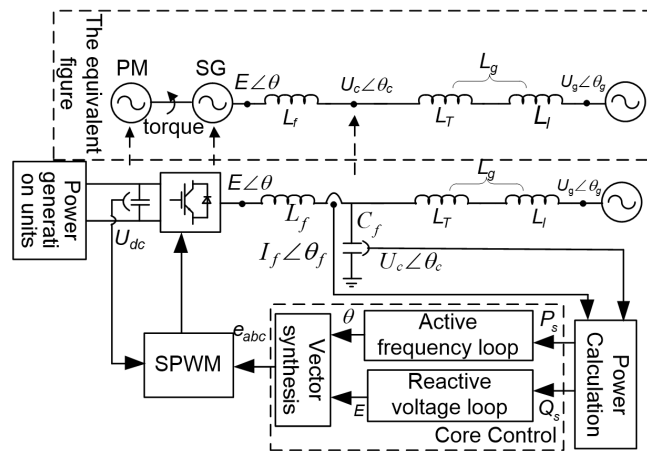


Fig. 1. Grid connection topology of VSG and its equivalent relation

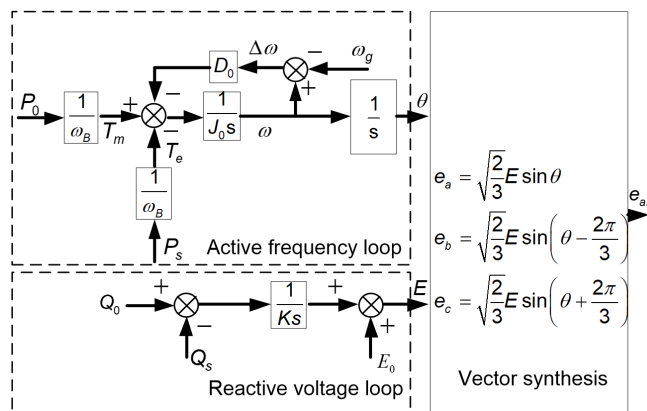


Fig. 2. Control strategy of VSG considering only the core control loop

synthesized to obtain the three-phase voltage of the VSG. The control strategy is established on the principle of the SG, by simulating the rotor swing equation to provide inertia and damping for the system. The corresponding expression is

$$\begin{cases} J_0 \frac{d\omega}{dt} = T_m - T_e - D_0 \Delta\omega = \frac{P_0 - P_s}{\omega_B} - D_0 \Delta\omega \\ \frac{d\theta}{dt} = \omega \end{cases}, \quad (2)$$

where: $\omega_B = 314$ rad/s is the rated angular velocity; P_0 and P_s are the active command at the rated angular frequency and the instantaneous active power; T_m and T_e are the equivalent mechanical torque and the equivalent electromagnetic torque; J_0 represents the virtual rotational inertia of

the VSG, which is the same as that of the SG; D_0 represents the damping coefficient of the VSG, which is related to the capacity of the VSG [22].

From the outlet inductor current $I_f \angle \theta_f$ and capacitor voltage $U_c \angle \theta_c$, P_s is

$$P_s = i_a u_a + i_b u_b + i_c u_c = \frac{EU_g}{X} \sin \delta, \quad (3)$$

where: i_a , i_b and i_c are the three-phase instantaneous currents corresponding to $I_f \angle \theta_f$; u_a , u_b and u_c are the three-phase instantaneous voltages corresponding to $U_c \angle \theta_c$, and X is the total equivalent impedance corresponding to the inductors L_g and L_f .

3. Mathematical model of the main loops of VSG

3.1. Virtual governor and virtual exciter

In SG control, the governor differs the output angular velocity ω_G from the rated angular velocity ω_B to obtain the deviation $\Delta\omega_G$. This value will be input to the governor, whose back stage is the PM, to adjust the SG frequency by changing the mechanical power transmitted from the PM to the SG. The active power reference value P_{Gm} is

$$P_{Gm} = P_{G0} - m \cdot \frac{1}{T_i s + 1} \cdot (\omega_G - \omega_B), \quad (4)$$

where: m is the frequency modulation coefficient; P_{G0} is the active power command at rated angular velocity, and T_i is the time constant of primary frequency modulation.

It can be seen from Eq. (4) that the SG frequency regulation time is generally long due to T_i . However, the virtual governor belongs to power electronic control, whose regulation process is very quick [20]. The corresponding active power reference value P_m is

$$P_m = P_0 - k_p (\omega - \omega_B), \quad (5)$$

where: P_0 is the active power command at the rated angular speed of the VSG; k_p is the frequency modulation coefficient, whose value is flexible. The control block diagram is shown in Fig. 3.

The composition of the virtual exciter is similar to that of the virtual governor, and its reactive power reference value Q_m is

$$Q_m = Q_0 - k_q (E - E_0), \quad (6)$$

where: E_0 is the rated internal potential; Q_0 is the reactive power command at the rated internal potential of the VSG; k_q is the voltage regulation coefficient, whose value is flexible. The control block diagram is shown in Fig. 4.

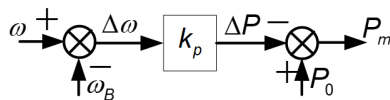


Fig. 3. Control block diagram of virtual governor

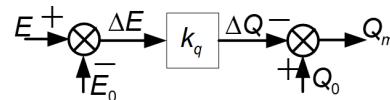


Fig. 4. Control block diagram of virtual exciter

3.2. Power filters

The VSG collects P_s and Q_s as input to the core control loop. Ideally, the power signal is constant for the fundamental voltage and current, but in practice, it is susceptible to ripple caused by interference. Therefore, power filters are usually introduced. Although the common filter is a second-order low-pass filter, to simplify the analysis, a first-order low-pass filter is used as an example in reference [21], and its transfer function is

$$H(s) = \frac{1}{\tau s + 1}, \quad (7)$$

where $\tau = RC = \frac{1}{2\pi f_c}$ is the time constant of the filter and f_c is the cut-off frequency.

Since the input and output of the active power filter are P_s and $P_{s,\text{filter}}$, according to (7), the time domain expression of the active power filter is

$$\tau \frac{dP_{s,\text{filter}}}{dt} + P_{s,\text{filter}} = P_s. \quad (8)$$

The reactive power filter is similar and the time domain expression is

$$\tau \frac{dQ_{s,\text{filter}}}{dt} + Q_{s,\text{filter}} = Q_s, \quad (9)$$

where Q_s and $Q_{s,\text{filter}}$ are the input and output of the reactive power filter. After power filtering, the interference can be significantly suppressed. However, from Eq. (3), it is known that the rms voltage drop of the infinity system leads to a sudden power change. During this period, the response characteristics and time delay of the power filter will have an impact on the synchronization stability of the VSG, which can be demonstrated in the later analysis.

3.3. Virtual impedance control

In the grid-connected structure of the VSG and infinity system, the current on the transmission line can be expressed as

$$\frac{E \angle \theta - U_g \angle \theta_g}{j(X_f + X_g)}. \quad (10)$$

When U_g drops severely, the VSG will generate an overcurrent. Different from the SG capable of withstanding overcurrents, the VSG contains numerous power electronics, and excessive current will result in breakdown. Thus, an appropriate control strategy to limit the fault current is needed [10]. At present, the current limiter and virtual impedance control are the main methods. Among them, the current limiter works on the current inner loop and virtual impedance control works on the voltage outer loop. This paper takes virtual impedance control as an example. When the fault current exceeds the threshold value I_{thr} , the virtual impedance Z_{virtual} will be put in. To simplify the analysis, this paper ignores the virtual resistance and only takes the virtual reactance X_{virtual} . When a fault occurs, the transmission line current expression after considering virtual impedance control is

$$\frac{E \angle \theta - U_g \angle \theta_g}{j(X_f + X_g + X_{\text{virtual}})}. \quad (11)$$

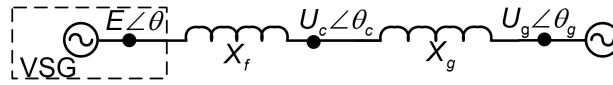


Fig. 5. Equivalent circuit diagram without considering virtual impedance

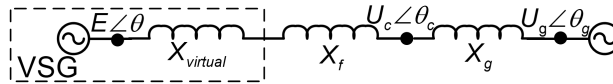


Fig. 6. Equivalent circuit diagram considering virtual impedance

Figures 5 and 6 give the equivalent circuits of the VSG and infinity system with and without considering virtual impedance, respectively.

In Fig. 7, P_{\max} , P'_{\max} and P''_{\max} are the limit power at a pre-fault steady state, a post-fault without virtual impedance, and a post-fault with virtual impedance, respectively. The expressions are

$$P_{\max} = \frac{EU_g}{X_f + X_g}, \quad P'_{\max} = \frac{EU_{g,\text{fault}}}{X_f + X_g}, \quad P''_{\max} = \frac{EU_{g,\text{fault}}}{X_f + X_g + X_{\text{virtual}}}, \quad (12)$$

where $U_{g,\text{fault}}$ is the rms value of the infinite system fault voltage. Since $P''_{\max} < P'_{\max}$, virtual impedance control will have an impact on the synchronization stability of the VSG.

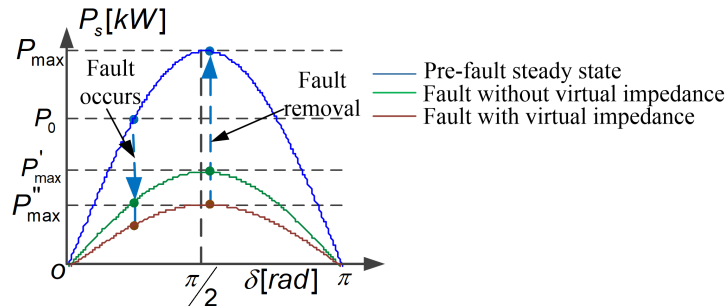


Fig. 7. Power angle curve of grid voltage drop and restoring

4. Mathematical model of VSG with integrated consideration of multiple control loops

4.1. Control strategy

In summary, after considering the virtual governor and virtual exciter, power filters and virtual impedance control, the core control of Fig. 1 becomes Fig. 8, with the red dotted box being the added control loops. In the fault current detection link, when the fault current exceeds I_{thr} , the control strategy shifts from “1” to “0” and puts in virtual impedance.

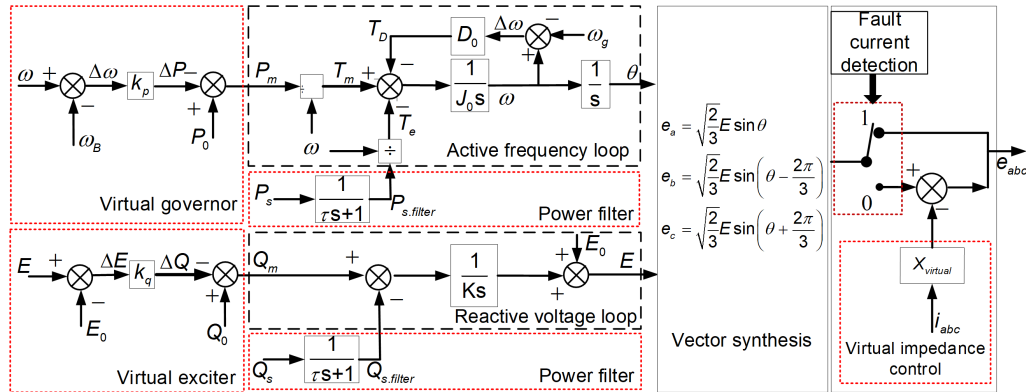


Fig. 8. Control strategy of VSG considering multiple control loops

4.2. The correlation formula between power angle difference and control parameters

In this paper, there are three assumptions in the mathematical model of the VSG: 1) the effect of the virtual exciter and the reactive voltage loop on the transient synchronization stability is neglected because this loop contains an integral link that makes the output voltage response slower [10]; 2) the grid-side frequency is a constant during the transient process, i.e., $\omega_g = \omega_B$; 3) the current flowing in the capacitor at the outlet of the VSG is ignored during the transient process.

The second-order rotor swing equation corresponding to active frequency loop in Fig. 9 is

$$J_0 \frac{d\omega}{dt} = T_m - T_e - T_D, \quad T_m = \frac{P_m}{\omega}, \quad T_e = \frac{P_{s.filter}}{\omega}, \quad T_D = D_0 (\omega - \omega_g), \quad \frac{d\theta}{dt} = \omega. \quad (13)$$

When substituting the terms 2, 3 and 4 into the term 1 of Eq. (13) we get

$$J_0 \frac{d\omega}{dt} = \frac{P_m - P_{s.filter}}{\omega} - D_0 \Delta\omega, \quad \frac{d\theta}{dt} = \omega, \quad (14)$$

where $P_{s.filter}$ represents the effect of the power filter on the equivalent electromagnetic torque.

From assumption (2) $\omega_g = \omega_B$, we have

$$\frac{d\omega}{dt} = \frac{d(\omega - \omega_B)}{dt} = \frac{d(\omega - \omega_g)}{dt} = \frac{d\Delta\omega}{dt}. \quad (15)$$

Substitute Eq. (15) into the term 1 of Eq. (14),

$$J_0 \frac{d\Delta\omega}{dt} = \frac{P_m - P_{s.filter}}{\omega} - D_0 \Delta\omega. \quad (16)$$

Then substitute Eq. (5) into Eq. (16) to obtain

$$\begin{aligned}
 J_0 \frac{d\Delta\omega}{dt} &= \frac{P_0 - k_p(\omega - \omega_B) - P_{s.\text{filter}}}{\omega} - D_0\Delta\omega \\
 &= \frac{P_0 - P_{s.\text{filter}}}{\omega} - \left[\frac{k_p(\omega - \omega_B)}{\omega} + D_0\Delta\omega \right] \\
 &= \frac{P_0 - P_{s.\text{filter}}}{\omega} - \left(D_0 + \frac{k_p}{\omega} \right) \Delta\omega \\
 &= \frac{P_0 - P_{s.\text{filter}}}{\omega} - D\Delta\omega,
 \end{aligned} \tag{17}$$

where $D = D_0 + \frac{k_p}{\omega}$ is the equivalent damping coefficient, and it reflects the primary frequency regulation characteristics of the virtual governor.

In order to study the variation of δ , take the derivation of Eq. (1) again

$$\ddot{\delta} = \frac{d^2\delta}{dt^2} = \frac{d\Delta\omega}{dt}. \tag{18}$$

When substituting Eq. (1) and Eq. (18) into Eq. (17), we have

$$J_0\ddot{\delta} = J_0 \frac{P_0 - P_{s.\text{filter}}}{\omega_B} - D\dot{\delta}. \tag{19}$$

The above equation is the mathematical model of the VSG considering multiple control loops, where $P_{s.\text{filter}}$ reflects the effect of the power filter on the equivalent electromagnetic torque; D reflects the effect of the virtual governor on the equivalent damping factor. The effect of virtual impedance control is indirectly reflected through the first-order differential equation of $P_{s.\text{filter}}$, which is obtained by transfer function (8)

$$\frac{dP_{s.\text{filter}}}{dt} = \frac{1}{\tau} (P_s - P_{s.\text{filter}}). \tag{20}$$

Substitute Eq. (3) into Eq. (20) to get

$$\frac{dP_{s.\text{filter}}}{dt} = \frac{1}{\tau} \left(\frac{EU_g}{X} \sin \delta - P_{s.\text{filter}} \right). \tag{21}$$

Equation (21) shows that the impedance in steady-state operation is between the VSG and infinite system, i.e., $X = X_f + X_g$. During the transient process, virtual impedance is introduced due to the overcurrent limit, and the impedance is the sum of steady-state impedance and virtual impedance, i.e., $X = X_f + X_g + X_{\text{virtual}}$. Therefore, X_{virtual} affects the variation of $P_{s.\text{filter}}$.

4.3. Control block diagram

In this paper, the power angle difference of the VSG-infinite system control block diagram in Fig. 8 can be reduced to Fig. 9 by combining Eq. (19) and Eq. (21).

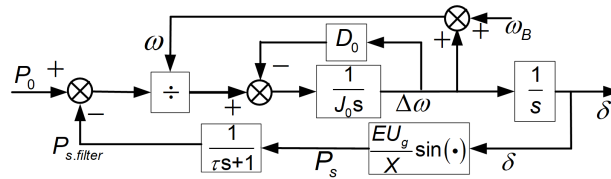


Fig. 9. Control block diagram of power angle difference of VSG-infinite system

5. Analysis of synchronization stability of VSG based on phase plane method

5.1. Analysis process

Equation (19) gives the power angle difference of the VSG-infinite system, a second-order nonlinear differential equation and it is difficult to find an analytical solution. In this paper, the phase plane method is introduced to determine the synchronization stability of the VSG according to the convergence or divergence characteristics of the phase trajectory.

For a second-order system, the plane $x_1 - x_2$ represented by the right-angle coordinate system formed with the phase variable

$$\begin{cases} x_1 = x \\ x_2 = \dot{x} \end{cases}$$

as the coordinate axis, is called the phase plane. The horizontal coordinate represents the state variable, and the vertical coordinate represents the first-order derivative of the state variable.

In order to analyze the synchronization stability of the VSG,

$$\begin{cases} x_1 = \delta \\ x_2 = \dot{\delta} = \Delta\omega \end{cases}$$

is taken as the phase variable, then the mathematical model of the VSG can be expressed as first order differential equations:

$$\begin{cases} \dot{x}_1 = x_2 \\ \dot{x}_2 = \frac{1}{J_0} \left(\frac{P_0 - P_{s.filter}}{x_2 + \omega_B} - D x_2 \right) \end{cases} \quad (22)$$

The additional equation is

$$\dot{P}_{s.filter} = \frac{1}{\tau} \left(\frac{EU_g}{X} \sin x_1 - P_{s.filter} \right) \quad (23)$$

The process of the phase plane method to evaluate the synchronization stability of the VSG is shown in Fig. 10, where t_{end} is the cut-off time of numerical calculation; Ode45 is a 4–5 order Runge–Kutta algorithm.

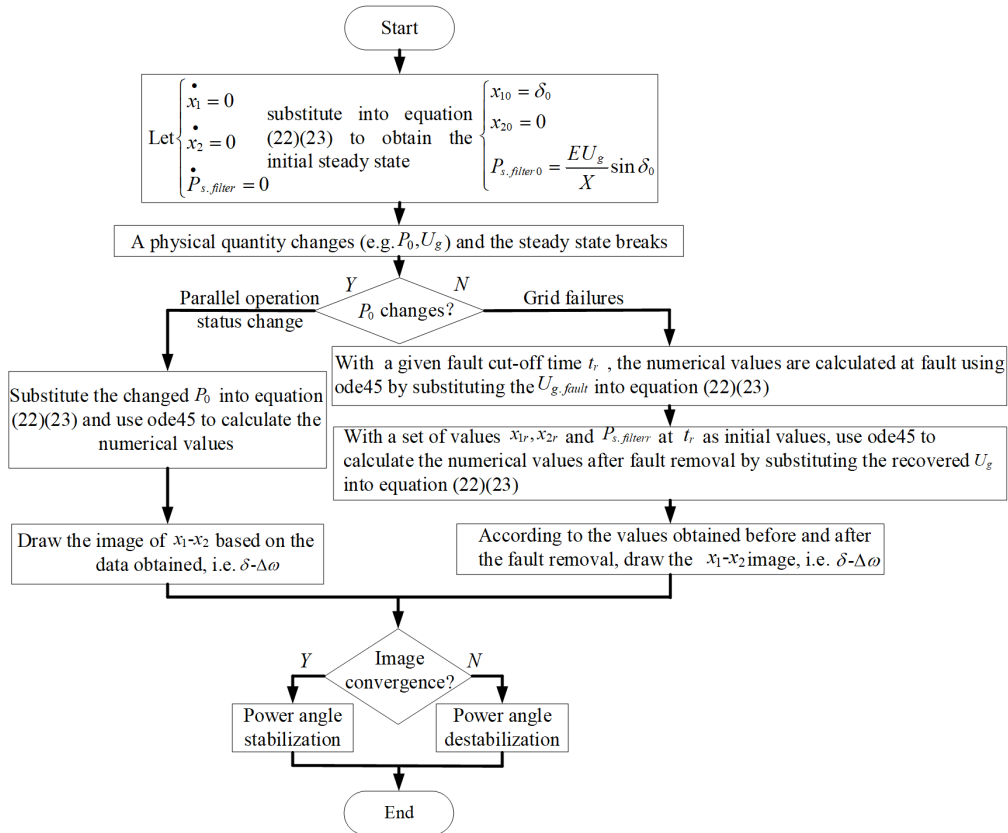


Fig. 10. Flow chart of phase plane method

5.2. VSG control parameters selection

1. Virtual inertia

The rotational inertia of the SG represents the inertia of the mechanical rotor when it rotates around its axis, expressed as

$$J_G = \frac{2HS_N}{\omega_B^2}, \quad (24)$$

where H is the inertia time constant and S_N is the rated capacity. Substitute $H = 2.5 \sim 10$ s [10] of the conventional turbine into Eq. (24) and the value range of J_0 is obtained as $(5.07 \times 10^{-5} S_N, 2.02 \times 10^{-4} S_N)$. Considering that the VSG simulates the operating characteristics of the SG, the same virtual inertia as that of the SG can be used [9], i.e., $J_0 = J_G$.

2. Damping coefficient and frequency modulation coefficient

The damping of the VSG is closely coupled to the virtual governor [5], and the equivalent damping coefficient $D = D_0 + k_p/\omega$ simulates the primary frequency modulation characteristics

of the SG with the ability to suppress the power grid oscillations. Among them

$$D_0 = \frac{100\%S_N}{\eta\% \omega_B^2}. \quad (25)$$

According to the reference [22], the conventional VSG angular speed adjustment range, taken as $\eta\% = 3\% \sim 5\%$, is substituted into Eq. (25) to obtain the setting range of D_0 as $(2.03 \times 10^{-4} S_N, 3.38 \times 10^{-4} S_N)$. According to the Technical Requirements for Connecting Photovoltaic Power System to Distribution Network, the power generation system should be able to operate normally when the frequency of the grid connection is $49 \sim 51$ Hz [19]. Therefore, the virtual governor is usually adjusted with 100% active power variation and $2\% \sim 0.5\%$ frequency variation (i.e., $1 \text{ Hz} \sim 0.25 \text{ Hz}$), which gives

$$k_p = \frac{100\%S_N}{(2\% \sim 0.5\%) \omega_B}. \quad (26)$$

3. Time constant of power filter

The cut-off frequency f_c of the power filter is usually several Hertz, and the time constant τ is

$$\tau = \frac{1}{2\pi f_c}. \quad (27)$$

In the paper, we take $f_c = 2 \text{ Hz} \sim 5 \text{ Hz}$ [21], so the value range of τ is $(1.59 \times 10^{-2} \text{ s}, 7.96 \times 10^{-2} \text{ s})$.

4. Virtual impedance

Since the inner electric potential in the VSG remains the same before and after the fault, the line current change after the fault is

$$|\Delta I| = \frac{|\Delta U_g|}{X_f + X_g + X_{\text{virtual}}}, \quad (28)$$

where ΔU_g is the grid voltage variation.

According to reference [10], the impedance between the VSG and the infinite system satisfies $X_f + X_g \ll X_{\text{virtual}}$. Then, Eq. (28) can be approximated as

$$|\Delta I| \approx \frac{|\Delta U_g|}{X_{\text{virtual}}}. \quad (29)$$

When the most severe voltage dip is encountered, the grid voltage is $U_g = 0$, $|\Delta U_g| = 1 \text{ pu}$. To ensure that the VSG output current is always within the tolerance range, take the line current $I \leq 1.3 \text{ pu}$, then $|\Delta I| \leq 0.3 \text{ pu}$ [10]. Substituting $|\Delta U_g|$ and $|\Delta I|$ into Eq. (29) yields

$$X_{\text{virtual}} = \frac{|\Delta U_g|}{|\Delta I|} = \frac{1 \text{ pu}}{0.3 \text{ pu}} = 3 \text{ pu}. \quad (30)$$

5.3. Analysis on synchronization stability of VSG during grid-connected operation

The common distributed energy sources are wind power or photovoltaic power, which are affected by wind and light, and the output power is random and fluctuating. Therefore, the active

power command P_0 of the VSG needs to be adjusted at the right time. In this paper, three cases are considered: P_0 decreases, P_0 increases, and P_0 increases to a special case above the limit power in steady-state operation. The parameters of the VSG-infinite system are shown in Table 1, substituting them into Eqs. (30) and (12), then obtaining $X_{\text{virtual}} = 28.88 \Omega$ and $P_{\text{max}} = 30.66 \text{ kW}$.

Table 1. Electrical parameters of VSG and line

Parameters	Values
Rated capacity S_N/kVA	15
Rated power P_N/kW	12
DC voltage U_{dc}/V	600
Equivalent internal potential E/V	380
Grid voltage U_g/V	380
Filter inductor L_f/mH	5
Line and transformer equivalent inductance L_g/mH	10

Assume that the initial steady-state operation of the VSG is $P_0 = P_N$. The control parameters are taken as $J_0 = 0.76 \text{ kg}\cdot\text{m}^2$, $D = 5.07 \text{ W}\cdot\text{m}^2/\text{rad}$ and $\tau = 31.8 \text{ ms}$. According to Fig. 10, the initial steady-state condition is obtained as $x_{10} = 0.128\pi$, $x_{20} = 0$ and $P_{s.\text{filter}} = 12 \text{ kW}$ by substituting $\dot{x}_1 = 0$, $\dot{x}_2 = 0$, and $\dot{P}_{s.\text{filter}} = 0$ into Eqs. (22) and (23).

When P_0 drops from P_N to $0.4P_N$, after substituting the changed P_0 into Eqs. (22) and (23) to calculate the first set of values, apply ode45 to Eqs. (22) and (23) to obtain $x_1 - x_2$ image, i.e., $\delta - \Delta\omega$. As shown in the red solid curve in Fig. 11, it is the convergence and δ that stabilize at a smaller value. When P_0 rises from P_N to $1.5P_N$, the phase trajectory $\delta - \Delta\omega$ is shown as the green dashed curve in Fig. 11, which represents the convergence and δ stabilized at a large

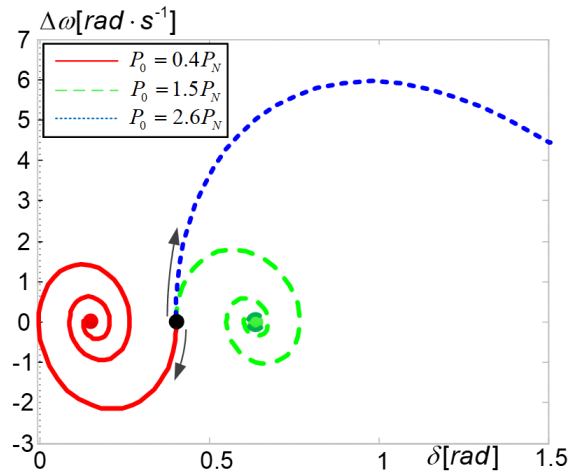


Fig. 11. Phase trajectories with different values of P_0

value. When P_0 rises from P_N to $2.6P_N > P_{max}$, the phase trajectory $\delta - \Delta\omega$ is shown as the blue dotted curve in Fig. 11. $\Delta\omega$ shows a large offset, and δ gradually becomes larger. Finally, the VSG becomes out of step.

According to the analysis in this paper, when the control parameters J_0 , D and τ are taken within a reasonable range, whenever the active power command P_0 exceeds the steady-state limit power P_{max} , it will cause the VSG to oscillate out of step.

5.4. Transient synchronization stability analysis of VSG

5.4.1. The impact of J_0

The initial operating state of the VSG still takes $P_0 = P_N$, $x_{10} = 0.128\pi$, $x_{20} = 0$ and $P_{s.filter} = 12$ kW. The control parameters $D = 4.05$ W·m²/rad, $\tau = 31.8$ ms and $X_{virtual} = 28.88$ Ω.

J_0 is taken as 3.03 kg·m² and 0.76 kg·m² for analysis, respectively. When the grid fault U_g falls from U_N to $0.3U_N$ and the fault removal time is taken as $t_r = 0.4$ s, the phase trajectory $\delta - \Delta\omega$ from fault occurrence to fault removal is derived as shown in the deep red solid curve and the deep blue one in Fig. 12, respectively, according to the analysis process in Fig. 10. Then U_g reverts to U_N after the fault is removed, corresponding to the phase trajectory $\delta - \Delta\omega$ as shown by the light red dotted curve and the light blue one in Fig. 12. The red curve shows convergence and the blue curve shows divergence. It indicates that the larger J_0 is, the better the transient synchronization stability of the VSG; otherwise, the VSG out-of-step phenomenon will occur. However, if J_0 is too large, δ will oscillate for a long time during the transition process.

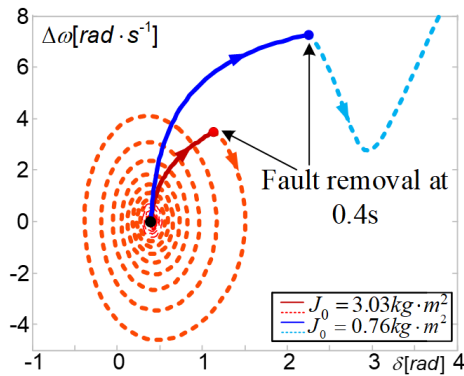


Fig. 12. Phase trajectory of grid voltage sag and recovery

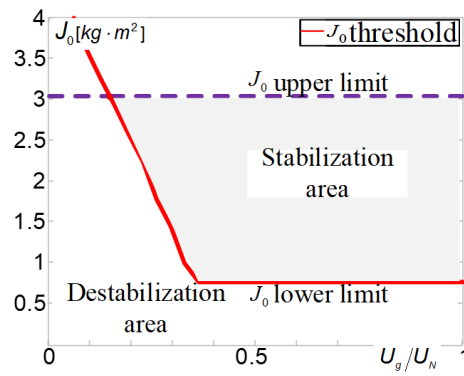


Fig. 13. The critical value of J_0 , assuming all other parameters remain the same

The relationship between the critical value of J_0 and U_g for the transient synchronization stability of the VSG is shown in Fig. 13. The region above the red curve is the stable region and that below the red curve is the unstable region. It can be seen that, with other control parameters unchanged, the more severe the drop of U_g is, the larger the requirement of J_0 is; when U_g falls seriously near $0.15U_N$, the conventional J_0 value cannot maintain the synchronization stability, and the adjustment of other parameters are needed.

5.4.2. The impact of D and the setting principle of k_p

1. The impact of D

The initial operation state of the VSG is the same as 5.4.1; the control parameters are taken as $J_0 = 0.76 \text{ kg}\cdot\text{m}^2$, $\tau = 31.8 \text{ ms}$, $X_{\text{virtual}} = 28.88 \Omega$. Take D as $5.07 \text{ W}\cdot\text{m}^2/\text{rad}$, and $3.05 \text{ W}\cdot\text{m}^2/\text{rad}$, respectively, for analysis. Figure 14 shows the phase trajectory $\delta - \Delta\omega$ when the grid fault U_g falls from U_N to $0.3U_N$ and the fault removal time is taken as $t_r = 0.4 \text{ s}$. The deep red solid curve and the deep blue one indicate the phase trajectory at fault. The light red dotted curve and the light blue one indicate the phase trajectory after fault removal. The red curve converges and the blue curve diverges. It indicates that the greater D is, the better the transient synchronization stability of the VSG is.

Equation (17) shows that D is the sum of k_p/ω and D_0 when considering the virtual governor, and D is positively correlated with k_p . Therefore, D can be improved by increasing k_p . However, in engineering, k_p cannot take arbitrarily large values due to hardware errors or controller accuracy limitations. Substituting the parameters of Table 1 into Eq. (26) yields $k_p \in (2388.54, 9554.14) \text{ W}\cdot\text{s}/\text{rad}$.

When other parameters remain unchanged, the critical value of D taken for the transient synchronization stability of the VSG versus U_g is shown in Fig. 15 with the stabilization region above the solid red curve and the destabilization region below. It can be seen that the stability region increases significantly after considering the virtual governor. However, according to the analysis in reference [22], too large D can slow down the response of the VSG and affect the control effect. The principle of taking k_p in engineering is studied below.

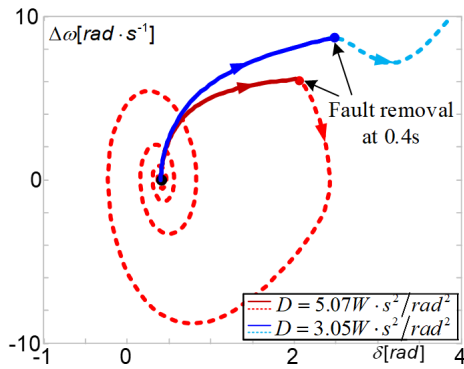


Fig. 14. Phase trajectory of grid voltage sag and recovery

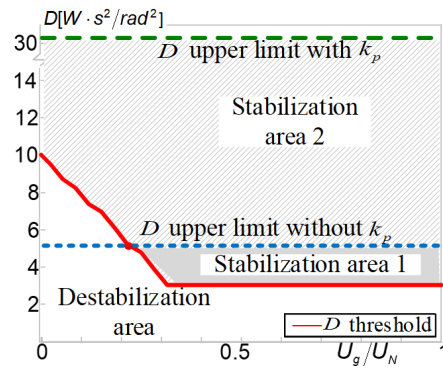


Fig. 15. The critical value of D , assuming all other parameters remain the same

2. The setting principle of k_p

The control system generally uses the “Siemens second-order optimal system” method to obtain a faster response and a smaller overshoot. The damping ratio of the second-order system is defined as 0.707, and the ideal D value versus J_0 is obtained as [23]

$$D = \frac{1}{\omega_B} \sqrt{\frac{2J_0\omega_B E U_g}{X}} \tag{31}$$

The ideal D value can be obtained by substituting the system parameters and control parameters into the above equation, and then the reasonable value of k_p can be obtained by $k_p \approx \omega_B(D - D_0)$. In the analysis of this paper, the ideal D value is calculated by substituting $J_0 = 0.76 \text{ kg}\cdot\text{m}^2$ into Eq. (28) as $12.18 \text{ W}\cdot\text{m}^2/\text{rad}^2$, which is located within the stabilization area 2 in Fig. 15. When D_0 is taken as $3.05 \text{ W}\cdot\text{m}^2/\text{rad}^2$, the corresponding $k_p \approx 2866.82 \text{ W}\cdot\text{s}/\text{rad}$. It can be seen that the reasonable adjustment of the k_p value can achieve both a good control effect and good response speed.

5.4.3. The impact of τ

The initial operation state of the VSG is the same as 4.4.1, and the control parameters are taken as $J_0 = 0.76 \text{ kg}\cdot\text{m}^2$, $D = 3.9 \text{ W}\cdot\text{m}^2/\text{rad}$, $X_{\text{virtual}} = 28.88 \Omega$. τ is taken as 79.6 ms and 15.9 ms for the analysis, respectively. The grid fault U_g falls from U_N to $0.3U_N$ and the fault removal time is taken as $t_r = 0.4 \text{ s}$. The phase trajectory $\delta - \Delta\omega$ is shown in Fig. 16 where the light red curve diverges and the light blue curve converges. It shows that the larger the τ is, the worse the transient synchronization stability of the VSG, due to the power signal time delay.

5.4.4. The impact of X_{virtual}

The initial operation state of the VSG is the same as 5.4.1, and the control parameters are taken as $J_0 = 0.76 \text{ kg}\cdot\text{m}^2$, $D = 4.05 \text{ W}\cdot\text{m}^2/\text{rad}$, $\tau = 31.8 \text{ ms}$. $X_{\text{virtual}} = 28.88 \Omega$ and $X_{\text{virtual}} = 0$ are taken for the analysis, respectively. The grid fault U_g falls from U_N to $0.3U_N$ and the fault removal time is taken as $t_r = 0.4 \text{ s}$. The phase trajectory $\delta - \Delta\omega$ is shown in Fig. 17 where the light red curve diverges and the light blue curve converges. It indicates that the introduction of X_{virtual} makes the transient synchronization stability worse and even an out-of-step phenomenon occurs. Theoretically, the virtual impedance makes the power angle curve at fault shift downward, and the acceleration area increases compared with that without virtual impedance, which is not conducive to synchronization stability, and it is consistent with the results of the phase plane analysis.

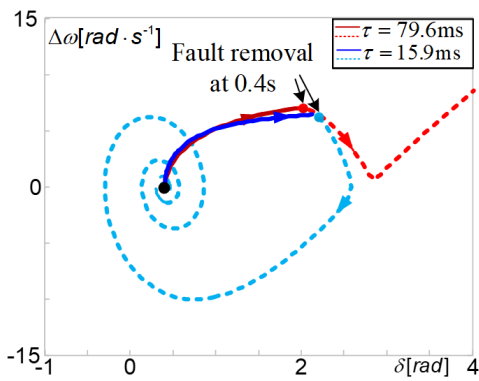


Fig. 16. Phase trajectory of grid voltage sag and recovery

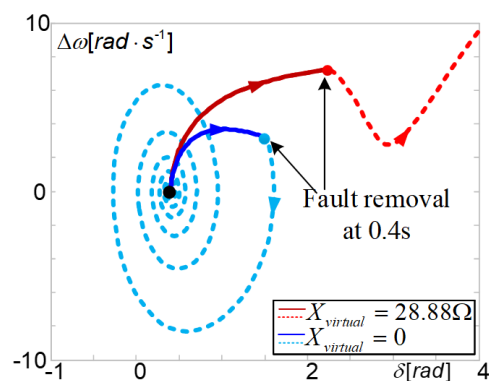


Fig. 17. Phase trajectory of grid voltage sag and recovery

6. Conclusion

This paper studies the influence of control parameters on the synchronization stability of the VSG, and draws the following conclusions.

1. In view of the current situation, where the control loops are not comprehensively considered in the research of the synchronization stability of the VSG, this paper establishes a VSG mathematical model comprehensively considering the virtual governor, the power filter and the current constraint control. On this basis, it deduces the correlation equation between the power angle difference and each control parameter.
2. Adopting the phase plane method, this paper studies the effects of main control parameters such as virtual inertia and damping coefficients of the active frequency loop, the frequency modulation coefficient of the virtual governor, time constant of power filters and the virtual impedance control of the VSG synchronization stability.
3. The VSG virtual inertia and equivalent damping coefficient increase in a reasonable range are beneficial to the transient synchronization stability, while the power signal time delay caused by the time constant of the power filter and the increase of impedance between the VSG and the infinite system caused by the virtual impedance are not conducive to the transient synchronization stability.
4. Considering that the introduction of the virtual governor increases the equivalent damping coefficient, starting with the virtual governor, our paper proposes the setting principle of the frequency modulation coefficient, which not only meets the response speed of control systems but also has a good control effect.

References

- [1] Su M., Dong H., Liu K., *Subsynchronous oscillation and its mitigation of VSC-MTDC with doubly-fed induction generator-based wind farm integration*, Archives of Electrical Engineering, vol. 70, no. 1, pp. 53–72 (2021), DOI: [10.24425/ae.2021.136052](https://doi.org/10.24425/ae.2021.136052).
- [2] Huang L., Xin H., Ju P., *Synchronization stability analysis and unified synchronization control structure of grid-connected power electronic devices*, Electric Power Automation Equipment, vol. 40, no. 9, pp. 10–25 (2020), DOI: [10.16081/j.epae.202009042](https://doi.org/10.16081/j.epae.202009042).
- [3] Xu Z., *Physical mechanism and research approach of generalized synchronous stability for power systems*, Electric Power Automation Equipment, vol. 40, no. 9, pp. 3–9 (2020), DOI: [10.16081/j.epae.202008009](https://doi.org/10.16081/j.epae.202008009).
- [4] Jin H., Luo Y., Fan Y., *Improved carrier phase shift modulation and voltage equalization control strategy in modular multilevel converter*, Archives of Electrical Engineering, vol. 68, no. 4, pp. 803–815 (2019), DOI: [10.24425/ae.2019.130684](https://doi.org/10.24425/ae.2019.130684).
- [5] Qi C., Wang K., Wu P., *Parameter space analysis of the rotor angle stability of virtual synchronous machine*, Proceedings of the CSEE, vol. 39, no. 15, pp. 4363–4373 (2019), DOI: [10.13334/j.0258-8013.pcsee.181280](https://doi.org/10.13334/j.0258-8013.pcsee.181280).
- [6] Pan D., Wang X., Liu F., Shi R., *Transient Stability Impact of Reactive Power Control on Grid-Connected Converters*, Proc. IEEE Energy Conversion Congress and Exposition (ECCE), Baltimore, MD, USA, pp. 4311–4316 (2019), DOI: [10.1109/ECCE.2019.8912567](https://doi.org/10.1109/ECCE.2019.8912567).
- [7] Wang X., Taul M.G., Wu H., Liao Y., Blaabjerg F., Harnefors L., *Grid Synchronization Stability of Converter-Based Resources – An Overview*, IEEE Open Journal of Industry Applications, vol. 1, pp. 115–134 (2020), DOI: [10.1109/OJIA.2020.302039](https://doi.org/10.1109/OJIA.2020.302039).

- [8] Huang L., Zhang L., Xin H., *Mechanism analysis of virtual power angle stability in droop-controlled inverters*, Automation of Electric Power Systems, vol. 40, no. 12, pp. 117–123 (2019), DOI: [10.7500/AEPS20150709007](https://doi.org/10.7500/AEPS20150709007).
- [9] Shuai Z., Shen C., Liu X., *Transient angle stability of virtual synchronous generators using lyapunov's direct method*, IEEE Transactions on Smart Grid, vol. 10, no. 4, pp. 4648–4661 (2018), DOI: [10.1109/TSG.2018.2866122](https://doi.org/10.1109/TSG.2018.2866122).
- [10] Hai H., *Research on Control Strategy of Distributed Virtual Co-generator under Non-ideal Operating Environment*, Metallurgical Industry Press (2020).
- [11] Qoria T., Gruson F., Colas F., Denis G., Prevost T., Guillaud X., *Critical clearing time determination and enhancement of grid-forming converters embedding virtual impedance as current limitation algorithm*, IEEE J. Emerg. Sel. Top. Power Electron., vol. 8, no. 2, pp. 1050–1061 (2020), DOI: [10.1109/JESTPE.2019.2959085](https://doi.org/10.1109/JESTPE.2019.2959085).
- [12] Qoria T., Gruson F., Colas F., Denis G., Prevost T., Guillaud X., *Current limiting algorithms and transient stability analysis of grid-forming VSCs*, Electric Power Systems Research, vol. 189 (2020), DOI: [10.1016/j.epsr.2020.106726](https://doi.org/10.1016/j.epsr.2020.106726).
- [13] Huang L., Xin H., Wang Z., Zhang L., Wu K., Hu J., *Transient Stability Analysis and Control Design of Droop-Controlled Voltage Source Converters Considering Current Limitation*, IEEE Transactions on Smart Grid, vol. 10, no. 1, pp. 578–591 (2019), DOI: [10.1109/TSG.2017.2749259](https://doi.org/10.1109/TSG.2017.2749259).
- [14] Zhao F., Shuai Z., Peng Y., *Evaluation method for transient stability of inverter containing current limiter*, Proceedings of the CSEE, vol. 41, no. 6, pp. 2245–2255 (2021), DOI: [10.13334/j.0258-8013.pcsee.200882](https://doi.org/10.13334/j.0258-8013.pcsee.200882).
- [15] Xiong X., Wu C., Hu B., Pan D., Blaabjerg F., *Transient Damping Method for Improving the Synchronization Stability of Virtual Synchronous Generators*, IEEE Transactions on Power Electronics, vol. 36, no. 7, pp. 7820–7831 (2021), DOI: [10.1109/TPEL.2020.3046462](https://doi.org/10.1109/TPEL.2020.3046462).
- [16] Xiong X., Wu C., Blaabjerg F., *An Improved Synchronization Stability Method of Virtual Synchronous Generators Based on Frequency Feedforward on Reactive Power Control Loop*, IEEE Transactions on Power Electronics, vol. 36, no. 8, pp. 9136–9148 (2021), DOI: [10.1109/TPEL.2021.3052350](https://doi.org/10.1109/TPEL.2021.3052350).
- [17] Wu H., Ruan X., Yang D., *Modeling of the Power Loop and Parameter Design of Virtual Synchronous Generators*, Proceedings of the CSEE, vol. 35, no. 24, pp. 6508–6518 (2015), DOI: [10.13334/j.0258-8013.pcsee.2015.24.027](https://doi.org/10.13334/j.0258-8013.pcsee.2015.24.027).
- [18] Zhu S., Liu K., Qin L., *Analysis of transient stability of power electronics dominated power system: an overview*, Proceedings of the CSEE, vol. 37, no. 14, pp. 3948–2962 (2017), DOI: [10.13334/j.0258-8013.pcsee.170366](https://doi.org/10.13334/j.0258-8013.pcsee.170366).
- [19] Lv Z., Sheng W., Liu H., *Application and challenge of virtual synchronous machine technology in power system*, Proceedings of the CSEE, vol. 37, no. 2, pp. 1–9 (2017), DOI: [10.13334/j.0258-8013.pcsee.161604](https://doi.org/10.13334/j.0258-8013.pcsee.161604).
- [20] Wang X., Huang C., Zhang J., Li C., *Analysis of Control Strategy of Microgrid Inverter Based on Virtual Synchronous Generator*, Electric engineering, vol. 12, pp. 45–47, 52 (2019), DOI: [10.19768/j.cnki.dgjs.2019.12.019](https://doi.org/10.19768/j.cnki.dgjs.2019.12.019).
- [21] Yan D., Guerrero J.M., Chang L., *Modeling, analysis, and design of a frequency-droop-based virtual synchronous generator for microgrid applications*, Ecce Asia Downunder, Melbourne, VIC, Australia, pp. 643–649 (2013), DOI: [10.1109/ECCE-Asia.2013.6579167](https://doi.org/10.1109/ECCE-Asia.2013.6579167).
- [22] Wang Y., Liu B., Duan S., Xu J., *Research on Transient Characteristic Optimization of Virtual Synchronization Generator Control Strategy*, Proceedings of the CSEE, vol. 39, no. 20, pp. 5885–5894 (2019), DOI: [10.13334/j.0258-8013.pcsee.182436](https://doi.org/10.13334/j.0258-8013.pcsee.182436).
- [23] Wu H., Ruan X., Yang D., *Modeling of the Power Loop and Parameter Design of Virtual Synchronous Generators*, Proceedings of the CSEE, vol. 35, no. 24, pp. 6508–6518 (2015), DOI: [10.13334/j.0258-8013.pcsee.2015.24.027](https://doi.org/10.13334/j.0258-8013.pcsee.2015.24.027).